

This is a non-peer-reviewed preprint submitted to EarthArXiv.

This manuscript has been submitted for publication in Geophysical Journal International. Please note the manuscript has yet to be formally accepted for publication. Subsequent versions of this manuscript may have slightly different content. If accepted, the final version of this manuscript will be available via the 'Peer-reviewed Publication DOI' link on the right-hand side of this webpage. Please feel free to contact any of the authors; we welcome feedback.

DeepSubDAS: An Earthquake Phase Picker from Submarine Distributed Acoustic Sensing Data

Han Xiao¹*, Frederik Tilmann^{1,2}, Martijn van den Ende³, Diane Rivet³,

Afonso Loureiro^{4,5}, Takeshi Tsuji⁶, Arantza Ugalde⁷, Qibin Shi⁸, Marine A. Denolle⁸

¹ Helmholtz Center Potsdam, German GeoResearch Center GFZ, Potsdam, Germany

Key words: DAS, Earthquake detection, Phase picking, Submarine cables, Deep learning

SUMMARY

Given the scarcity of seismometers in marine environments, traditional seismology has limited effectiveness in oceanic regions. Submarine Distributed Acoustic Sensing (DAS) systems offer a promising alternative for seismic monitoring in these areas. However, the existing machine learning model trained on land-based DAS data does not perform well with submarine DAS due to differences in noise characteristics, deployment conditions, and environmental factors. This study presents a machine learning approach tailored specifically to submarine DAS data to enable automated seismic event detection and P and S wave identification. Leveraging DeepLab v3, a neural network architecture opti-

² Institute for Geological Sciences, Freie Universität Berlin, Berlin, Germany

³ Université Côte d'Azur, CNRS, Observatoire de la Côte d'Azur, IRD, Géoazur, Sophia Antipolis, France

⁴ Agência Regional para o Desenvolvimento da Investigação, Tecnologia e Inovação, Funchal, Portugal

⁵ IDL - Instituto Dom Luiz, Faculdade de Ciências, Universidade de Lisboa, Lisboa, Portugal

⁶ School of Engineering, The University of Tokyo, Tokyo, Japan

⁷ Institute of Marine Sciences, ICM-CSIC, Barcelona, Spain

⁸ Department of Earth and Space Sciences, University of Washington, Seattle, WA, USA

^{*} Corresponding author: xiaohan@gfz.de

mized for semantic segmentation, we developed a specialized model to handle the unique challenges of submarine DAS data. Our model was trained and validated on a dataset comprising nearly 57 million manually and semi-automatically labeled seismic records from multiple globally distributed submarine sites, providing a robust basis for accurate seismic detection. The model adapts to a variety of deployment scenarios and can process DAS data from cables with different lengths, configurations, and channel spacings, making it versatile for various ocean environments. We thus provide an adaptable and efficient tool for automated earthquake analysis of DAS data, which has the potential to enhance real-time earthquake monitoring and tsunami early warning in submarine environments.

1 INTRODUCTION

In the last decade, distributed acoustic sensing (DAS) has advanced rapidly, transforming fiber optic cables into dense seismic sensor networks (Posey et al. (2000)). Its high spatial resolution, cost-effectiveness, and ease of deployment have expanded its applications across seismology (Lindsey et al. (2017); Jousset et al. (2018)). In addition, the volume of DAS data collected from submarine environments has increased significantly, driven by advances in fiber optic technology and its deployment in underwater settings (Lindsey et al. (2019); Sladen et al. (2019); Spica et al. (2023); Romanowicz et al. (2023); Shi et al. (2025)). This surge in data presents a unique opportunity to advance earth-quake detection and characterization in marine environments (Ugalde et al. (2021); Lior et al. (2023); Mata Flores et al. (2023); Strumia et al. (2024)). Better information on offshore earthquakes is invaluable for studies of fault behaviour, earhthquake physics and seismotectonics; this is of particular relevance in subduction zones where often most of the plate interface seismicity occurs offshore and where existing studies frequently suffer from limited backazimuthal coverage. In addition, if submarine DAS data can be processed in real-time, additional lead time for earthquake and tsunami early warning could be achieved (Yin et al.) (2023); van den Ende et al.) (2025); Lior et al.) (2023)).

However, offshore seismic sensing is challenging due to the complex and often uncontrollable underwater environment, where acoustic signals from ocean dynamics overlap with those from tectonic activity. Traditional seismic detection methods for submarine environments, such as the STA / LTA (Short-Term Average / Long-Term Average) trigger algorithm and template matching, face significant challenges when applied to DAS data. The STA/LTA method is highly sensitive to noise and often results in false detections in marine environments due to microseisms, vessel noise, ocean waves, and marine life (Bouffaut et al. (2022); Xiao et al. (2022); Wilcock et al. (2023); Williams et al. (2023); Xiao et al. (2024)), which degrade the signal-to-noise ratio (SNR) of seismic signals (Withers et al.) (1998) and are often also transient. Template matching, while improving detection ac-

curacy, requires predefined waveform templates, making it less adaptable to the diverse and complex waveforms observed in submarine DAS recordings (Yoon et al. (2015)). At the same time, a non-linear azimuthal response in DAS must also be accounted for, which can further complicate seismic signal interpretation (Posey et al. (2000)). Denoising before detection, whether in the form of denoising (Shi et al. (2025)) or wavefield separation (Ni et al. (2024)), adds complexity to workflows. Furthermore, the shallow marine sediment layer introduces various converted waves, such as basement-converted PS waves, adding another layer of complexity to the signal interpretation (Spica et al. (2020); Trabattoni et al. (2024)). Meanwhile, the recently developed Kurtosis-Value-Picker (KVP) algorithm may improves seismic event detection and phase picking accuracy in complex DAS and OBS data using multiband kurtosis-based characteristic functions (Latorre et al. (2025)).

Recent advances in machine learning, especially deep learning, have shown promise in addressing these challenges, with studies demonstrating the efficacy of deep learning models in automatically detecting and classifying seismic events (Zhu & Beroza (2018); Zhu et al. (2023); Mousavi et al. (2019) (2020)). However, models trained in terrestrial seismic data often fail to perform adequately in submarine environments due to different noise characteristics and geological differences (Ruppert et al. (2022); Niksejel & Zhang (2024); Bornstein et al. (2024)). Currently, the vast majority of machine learning models are trained on data from traditional three-component seismometers, making them unsuitable for direct application to single-component DAS data

They are further impractical for large-scale deployment on DAS, either due to their reduced performance or to computational expense (Zhu & Beroza) (2018); Shi et al. (2025)). To our knowledge, currently there is only one model trained on DAS data, PhaseNet DAS, which is based on three terrestrial DAS datasets acquired in California, which limits its applicability in submarine environments (Zhu et al. (2023)). Recognizing these challenges, there is a clear need for specialized models capable of accurately labeling submarine DAS data.

To address these challenges, we propose training a deep learning model specifically on submarine DAS data. Specifically, we adapt the DeepLab model, which is known for its robust performance in image segmentation tasks, as a promising approach for seismic wave detection and classification in submarine environments (Chen et al. (2017)). The development of such a model has the potential to improve our understanding of submarine seismic activity and contribute to more effective earthquake monitoring and early warning systems (Yin et al.) (2023)).

In this study, we train our model using 57 million DAS records, which were collected from 6,314 seismic events across 13 submarine fiber optic cables worldwide. To build a robust training dataset, we developed an interactive semi-automated tool to label the P and S waves in DAS data. This tool improves the accuracy and efficiency of the labeling, creating high-quality manually labeled data essential for adapting DAS models to the complexities of the submarine environment. Through this

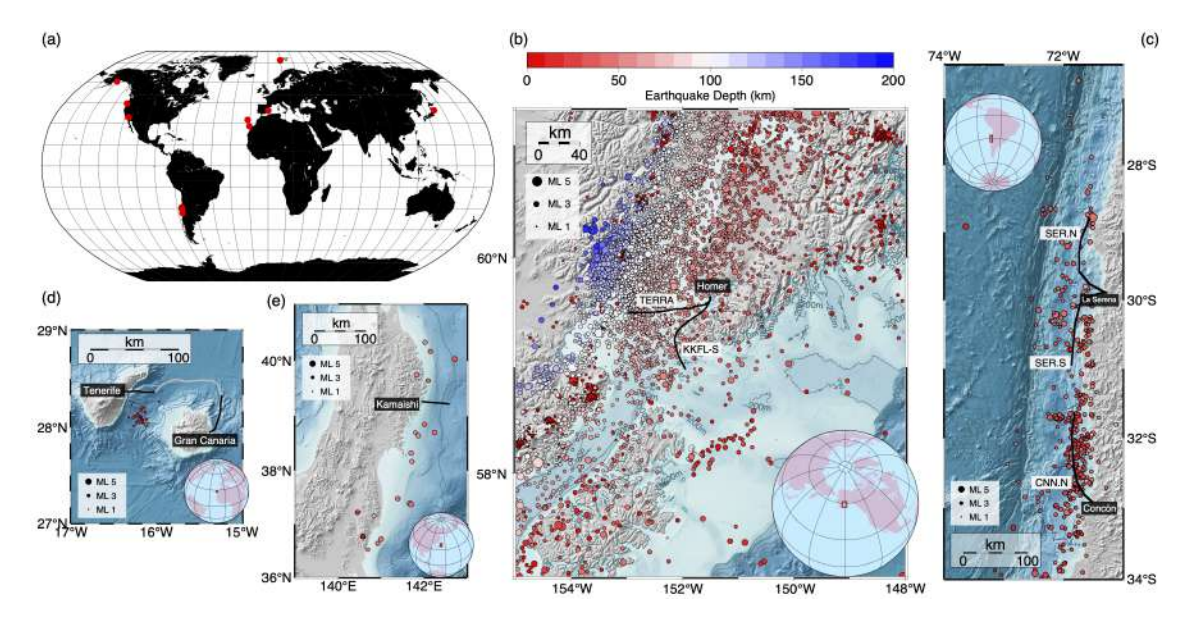


Figure 1. (a) Map showing the locations of all Distributed Acoustic Sensing (DAS) cables used in this study. Each red dot represents the position of a fiber optic cable. (b) The largest dataset is from the southern coastal region of Alaska, with two black lines marking the positions of the TERRA and KKFL-S DAS fibers. Earthquake locations are depicted by circles, with color indicating depth and size representing magnitude. (c) Another primary dataset comes from the Chilean coastline, where three cables CCN.N, SER.S, and SER.N are shown by black lines alongside earthquake locations. (d) The locations of two DAS cables and corresponding earthquake locations in the Canary Islands. (e) The DAS cable and earthquake locations in Kamaishi, Japan.

work, our goal is to advance seismic monitoring capabilities in underwater settings, bridging the gap between terrestrial and underwater DAS applications.

2 DATA AND MODEL

2.1 Curated DAS dataset

To ensure that our machine learning model applies to various oceanic environments worldwide, we have made a concerted effort to gather submarine DAS seismic data from multiple global locations. Our study uses DAS data collected from 13 submarine fiber optic cables around the world, covering nearly 92 million seismic records (Fig. Ta). Additionally, we incorporated land-based DAS earthquake records from the Ridgecrest region in California to pre-train our model. The following sections introduce the primary data sources and their key characteristics.

The first dataset, which is the largest data source, comes from two optical fibers along Alaska (Fig. []b) Shi et al. (2025). In June 2023, two submarine telecom cables were connected to a single Sintela Onyx v1.0 interrogator unit at the GCI Communication landing station in Homer, Alaska. The two fiber-optic cables include the southern span of the Kodiak Kenai Fiber Link (KKFL-S), oriented north-south, and the east-west oriented TERRA (Terrestrial for Every Rural Region in Alaska) cable. The strain recordings were decimated from a sampling rate of 1.25 kHz to 25 Hz to reduce storage

Table 1. Summary of DAS dataset statistics.

Location	Year	Region	Channel	Event No.	Records	Citation
KKFL-S/Homer	2024	Alaska	8,531	5,985	40 M	Shi et al. (2025)
TERRA/Homer	2024	Alaska	8,531	5,985	40 M	Shi et al. (2025)
CCN.N/La Serena	2021	Chile	36,718	41	1.5 M	Strumia et al. (2024)
CCN.N/La Serena	2023	Chile	15,000	229	3.4 M	van den Ende et al. (2025)
SER.S/Michilla	2023	Chile	15,000	229	3.4 M	van den Ende et al. (2025)
SER.N/Michilla	2023	Chile	15,000	229	3.4 M	van den Ende et al. (2025)
Tenerife	2020	Spain	5,984	28	0.17 M	Ugalde et al. (2021)
Gran Canaria	2020	Spain	5,984	28	0.17 M	Ugalde et al. (2021)
Kamaishi	2020	Japan	6,000	23	0.14 M	Tsuji et al. (2021)
Svalbard	2020	Norway	30,000	3	0.09 M	Bouffaut et al. (2022)
Valencia	2020	Spain	2,977	2	0.006 M	X1ao et al. (2022)
Florence	2021	Oregon	3,000	2	0.006 M	Xiao et al. (2024)
GeoLAB/Madeira	2023	Portugal	11,294	1	0.001 M	Loureiro et al. (2025)
Total	-	_	116,748	6,314 (Unique	92.0 M	-

demands. The channel spacing is 9.57 m, with a gauge length of 17.55 m from June to September and 23.93 m from September to December. Each cable spans 81.64 km, with 8531 channels in each DAS data array. During this period, nearly 6000 earthquakes occurred in the vicinity of 200 km, generating close to 80 million single-channel earthquake records (Fig. 14, Table 11). The earthquakes were detected by the United States Geological Survey Advanced National Seismic System as part of standard operations of the Alaska Earthquake Center network.

Fig. 2a shows the distribution of the SNR (db) for all seismic records. The SNR is defined here as the ratio between the maximum absolute amplitude of the seismic signal and the root-mean-square (RMS) amplitude of the noise in the 3 s preceding the event. The signal amplitude is determined based on manually labeled P and S wave arrival times: we extract a 1 s window centered around each arrival (0.5 s before and after) and use the maximum absolute value within that window. The signal arrival times are identified from manual picks and used directly to define the time window for each phase. This approach ensures that the SNR calculation accurately reflects the observed signal characteristics rather than relying on theoretical travel-time estimates.

As shown in Fig. 2a, the number of S wave records is more than double that of P wave records. In addition, the S wave generally has a slightly higher SNR compared to the P wave, with most S wave SNRs around 8, while the P wave SNRs are mostly around 6. Fig. 3a and Fig. 4a present the frequency of earthquake magnitudes and depths. The majority of earthquakes have magnitudes between 1 and 3, with depths less than 150 km.

The second largest dataset comes from three DAS recordings along the Chilean coastline (Fig. 1c). In November 2021, DAS data were recorded in Chile using an OptoDAS interrogator unit from Alcatel Submarine Networks. This unit was connected to a submarine fiber optic telecom cable operated by the GTD group, spanning from Concón to La Serena (CCN.N) (Strumia et al. (2024)). The DAS system monitored a 150 km-long segment of this cable. The data were initially recorded with an 8.16 m gauge

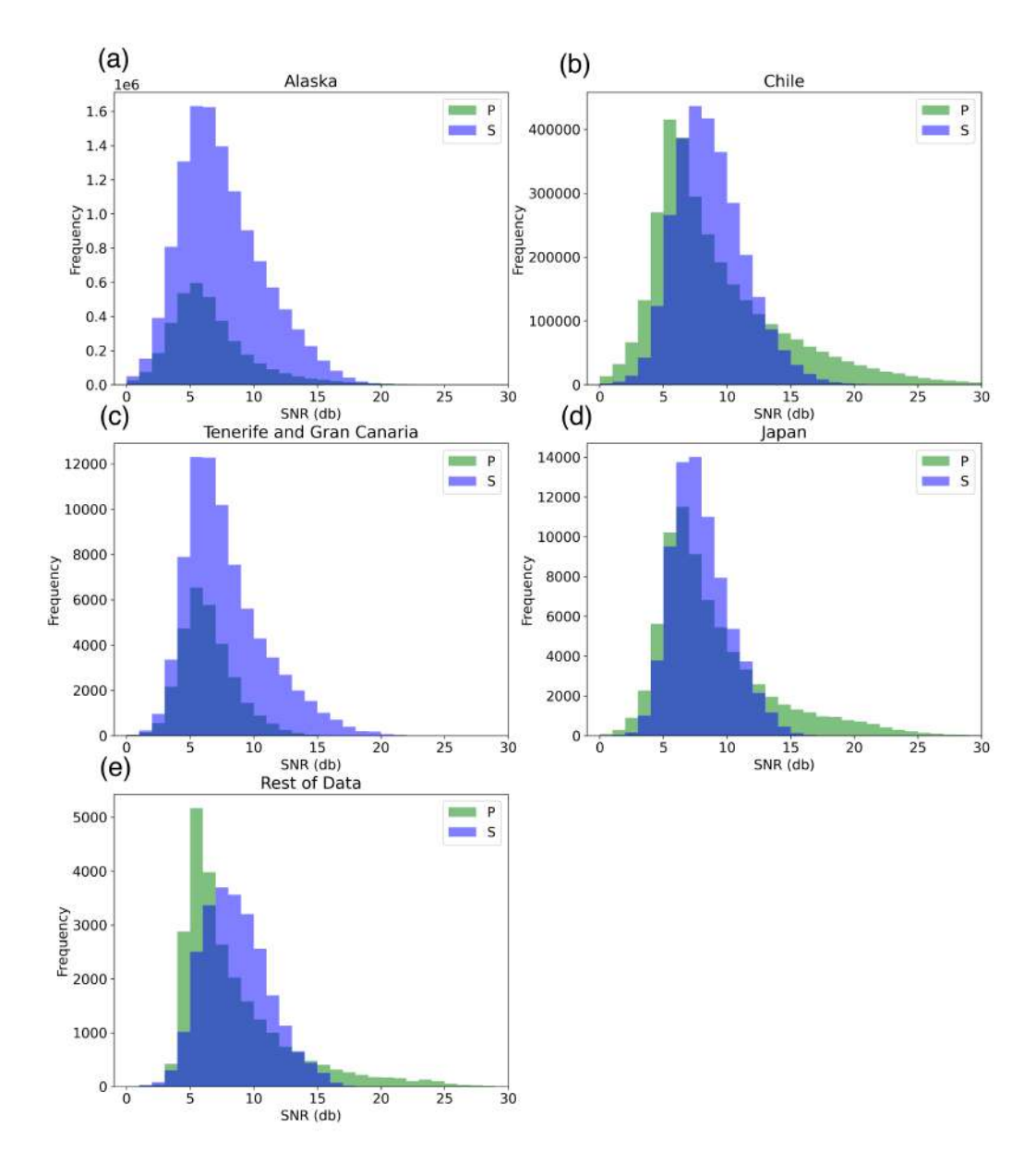


Figure 2. Signal-to-noise ratios (SNR (db)) of P wave and S wave recorded by seafloor DAS across various regions. Note that the SNR follows a decibel scale, i.e., a value of 20 corresponds to an SNR of 100. (a) The southern coastal region of Alaska. (b) The coastal region of Chile. (c) The area between Tenerife and the Gran Canaria Islands. (d) The offshore region in northeastern Japan. (e) The rest of the data.

length, a sampling rate of $625\,\mathrm{Hz}$, and a spatial sampling interval of $1.02\,\mathrm{m}$, averaged over $4.08\,\mathrm{m}$, resulting in a total of 36,718 channels. The data were later downsampled to a $125\,\mathrm{Hz}$ sampling rate. In total, we collected 41 earthquakes comprising $1.5\,\mathrm{million}$ seismic records.

In a subsequent experiment along the Chilean coast between 2023 and 2024, DAS data were acquired from three fiber optic cables running approximately parallel to the Chilean coastline for most of their span (van den Ende et al.) (2025)). The DAS system monitored three 150 km-long segments of

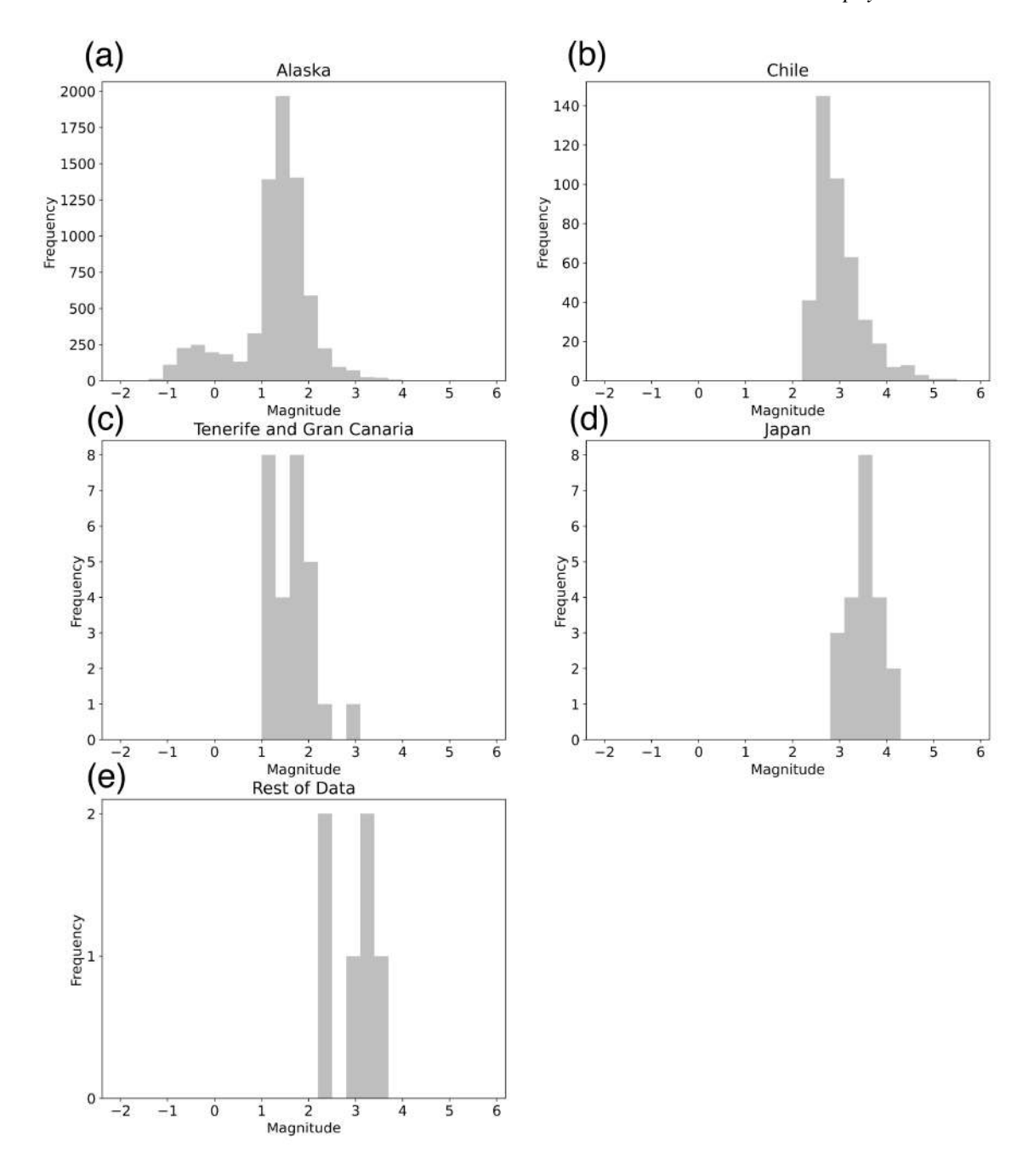


Figure 3. Earthquake local magnitude (ML) distribution. (a) The southern coastal region of Alaska. (b) The coastal region of Chile. (c) The area between Tenerife and the Gran Canaria Islands. (d) The offshore region in northeastern Japan. (e) The rest of the data.

these cables (CCN.N, SER.S, and SER.N) (Fig. 1c). The data were recorded with a spatial sampling interval of 10 m and a frequency of 125 Hz. It recorded 229 earthquakes during this period, resulting in 10 million seismic records across the three fibers. As shown in Fig. 2b, similar to the Alaska data, the S wave generally exhibits a higher SNR, with most S wave SNRs around 10, while most P wave

SNRs are around 6. However, P wave reaches the highest SNR values, with some exceeding 30. This may be related to our calculation method, as the noise preceding the P wave is relatively low, whereas the coda of the P wave can affect the SNR estimation for the subsequent S wave. Fig. 3b and 4b display the frequency distribution of earthquake magnitudes and depths. The majority of earthquakes in these datasets have magnitudes between 2 and 6 and are shallower than 100 km.

The third major dataset was collected from an undersea fiber-optic telecommunication cable that links the islands of Tenerife and Gran Canaria. Two DAS interrogators monitored 5,984 channels each, with a spatial resolution of 10 m (channel length), covering the first 60 km of fiber starting from the coastline and extending into the sea (Ugalde et al. (2021)). The data were initially recorded with a sampling frequency of 1 kHz and were later downsampled to 50 Hz. The DAS systems recorded 28 earthquakes, comprising 330,064 seismic records. In this dataset, the number of S wave records exceeds that of P wave, and the S wave also exhibits a significantly higher SNR (Fig. 2c). Similarly, Fig. 3c and Fig. 4c show the distribution of earthquake magnitudes and depths from these catalogs, with magnitudes ranging from 1 to 3 and depths down to 50 km.

The fourth dataset comes from the coast of Japan. We utilized DAS data recorded from the seafloor off the coast of Kamaishi, northeast Japan, collected between 10 October and 23 November 2020 (Tsuji et al.) (2021). In this test survey, the spatial sampling interval was set to 10 m, with a gauge length of 20 m. The cable used in this experiment was 60 km long, providing data from 6,000 channels. The sampling rate is 500 Hz in this offshore experiment. In total, it recorded 23 earthquakes, comprising 138,000 seismic records. The SNR of earthquakes in the Japan region is slightly lower than that along the Chilean coast although the magnitude distribution is similar (Fig. 3b and Fig. 3d), likely due to the larger epicentral distances of the earthquakes in this area. In general, all the recorded earthquakes are shallow earthquakes 0 km to 100 km (Fig. 4d).

We also utilized data from cables located in Svalbard (Bouffaut et al. (2022)), Oregon (Xiao et al. (2024)), and off the coast of Spain in the Mediterranean (Xiao et al. (2022)), as well as data from the GeoLAB fiber in Madeira (Loureiro et al. (2025)). However, since these locations recorded less than 5 earthquakes each, we only provide summarized descriptions of these datasets in the table. For more information on the seismic data from these locations, please refer to the previously published articles (Table 1).

To enhance our dataset and improve the stability of our model, we augmented the data by incorporating real oceanic DAS seismic noise. These noise samples were carefully selected, ensuring that they were recorded during periods without seismic events. We employed the kurtosis function to determine whether the noise contained any seismic signals.

The kurtosis K is calculated using the following formula:

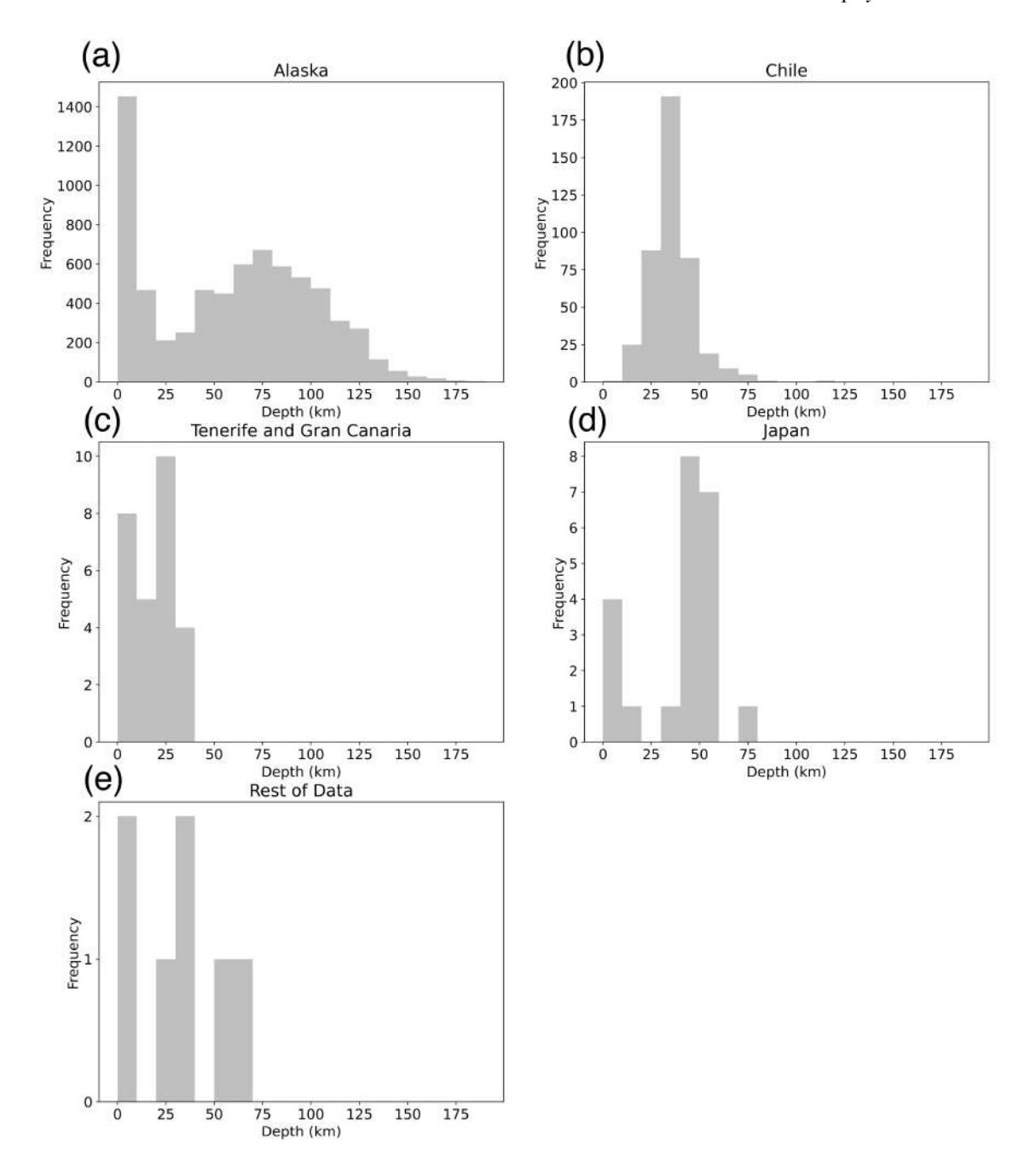


Figure 4. Earthquake depth distribution in the catalogs. (a) The southern coastal region of Alaska. (b) The coastal region of Chile. (c) The area between Tenerife and Gran Canaria Islands. (d) The offshore region in northeastern Japan. (e) The rest of the data.

$$K = \frac{\sum (x_i - \bar{x})^4}{n \cdot \sigma^4} - 3,$$

where x_i is the *i*-th data point in the dataset. \bar{x} is the mean of the dataset. n is the total number of samples in the dataset. σ is the standard deviation of the dataset. To maintain the coherence in the seis-

mic waveforms across different channels, we did not add noise to each channel individually. Instead, we added noise with the same array size to the earthquake waveforms in each patch. This method more closely mimics the conditions of our real seismic recordings, ensuring that the augmented data is more representative of actual DAS observations. Notably, these noise samples were sourced from various offshre DAS cables located around the world, further diversifying our dataset. Additionally, the noise was normalized, with levels randomly added ranging from 10% to 50% of signal amplitudes. This variability in noise levels enhances the robustness of our model by exposing it to different SNRs, ultimately improving its ability to detect small earthquakes.

2.2 Semi-automatic arrival time pick labelling

To ensure the quality and accuracy of our labeled data, we adopted a semi-automatic labeling approach. Initially, we applied PhaseNet (Zhu & Beroza (2018)), using the SeisBench (Woollam et al.) (2022); Münchmeyer et al. (2022)) platform, to perform single-channel labeling, leveraging its efficiency in identifying P and S seismic waves. We applied a band-pass frequency filter in the range of 0.5 Hz to 20 Hz, as well as an FK (frequency-wavenumber) filter with a slowness window corresponding to apparent velocities between $300\,\mathrm{m\,s^{-1}}$ and $50\,000\,\mathrm{m\,s^{-1}}$. Since PhaseNet is designed to take a three-component input, but DAS data contains only a single component, we duplicated the single DAS channel across all three input channels. We used the original pre-trained weights provided with PhaseNet. Whereas in many cases, this simplistic approach already resulted in reasonable picks, there were also many instances where the no arrival was identified, P and S waves were not identified correctly, or the wrong part of the waveform was picked (Shi et al.) (2025)). Therefore, to enhance the reliability of these labels, we developed an interactive software tool that allows manual correction of labeling results. We manually intervened every 5-10 channels, depending on the channel spacing for each DAS cable, correcting errors that might have arisen due to excessive noise on single-component DAS data (Fig. 5a). The arrival times of the P and S waves for the channels in between were determined through linear interpolation. We also conducted manual checks to ensure the accuracy of these interpolated times, and if any discrepancies were found, we intervened and corrected them manually (Fig. 5b). This hybrid method enabled us to efficiently and accurately label P and S wave seismic records, ensuring more accurate labeled data for subsequent analysis (Fig. 5c).

Due to the low SNR ratio in some DAS seismic data, there are instances where even manual labeling cannot accurately determine the P and S wave arrival times (SNR < 3). In such cases, we choose to discard this data to maintain the overall quality and accuracy of the dataset.

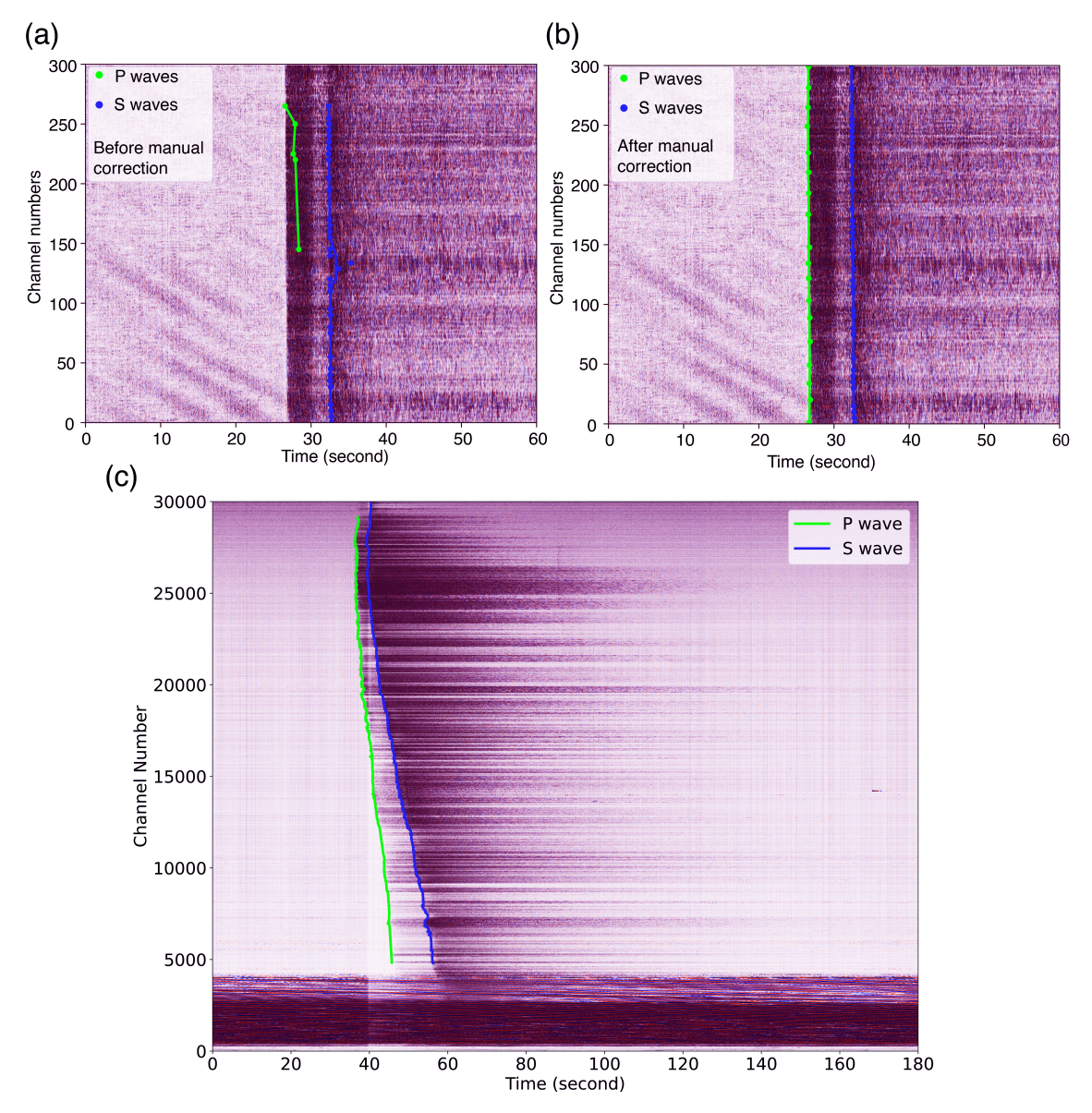


Figure 5. An example of semi-automatic labeling of P and S waves from the Chile dataset. (a) We initially labeled the P and S waves using PhaseNet from the SeisBench platform, (b) then manually corrected any mislabeled data through our interactive software tool (c) The final label result from this semi-automatic process.

2.3 Training dataset preparation

Only the highest-quality seismic records in the frequency range of $1 \,\mathrm{Hz}$ to $20 \,\mathrm{Hz}$, exhibiting clear waveforms and minimal noise interference, were selected for further analysis. This frequency range effectively minimizes the influence of ocean wave noise, which predominantly occurs below $0.2 \,\mathrm{Hz}$ (Lindsey et al.) (2019); Sladen et al. (2019); Xiao et al. (2024), and reduces interference from Scholte wave seismic noise, typically observed between $0.1 \,\mathrm{Hz}$ to $2 \,\mathrm{Hz}$ (Lindsey et al.) (2019); Sladen et al.)

(2019); Xiao et al. (2022)). Filtering within this range ensures the retention of critical seismic information while discarding irrelevant background noise.

To standardize the data for analysis and model training, we resampled all waveforms to a uniform rate of 100 Hz, aligning with typical requirements for seismic analysis (e.g., default sampling rate in SeisBench models) while maintaining sufficient temporal resolution for accurate signal interpretation. However, we preserved the original channel spacing of each DAS dataset to retain the different inherent spatial resolutions and specific characteristics of the seismic signals. This balance between standardization and preserving unique dataset properties is critical for ensuring the generalization of the model.

Subsequently, we extracted 40 s segments of earthquake waveforms, with the start time randomly chosen between 2 and 10 s before the manually picked P-wave arrival in the middle channel. This method aligns with established data preparation techniques and ensures that the extracted segments capture a mix of seismic signals and background noise. We also randomly added real DAS seismic noise chosen before to the earthquake data. Incorporating this noise is essential for training models capable of robust detection across a variety of SNR conditions. To ensure balanced representation in the training data, we exclusively selected earthquake records containing both P and S waves, enabling the model to effectively learn the characteristics of both phases.

The processed data were then organized into manageable patches consisting of 200 to 500 DAS channels, with the specific number determined by the spacing between the channels to ensure optimal segmentation for the dataset. For training purposes, we exclusively used labeled earthquake data within these patches to guarantee the model learns from well-defined examples, avoiding any inclusion of unlabeled segments.

2.4 Training data augmentation

To further augment the dataset, we applied slight temporal stretching and compression (less than 10%) along the time axis. This approach is inspired by techniques used in image segmentation, where geometric transformations are applied to introduce variability in the training data without altering its core features and has been successful for training phase pickers across a wide range of frequencies [Shi] & Denolle (2023). This technique simulates potential inter-channel timing variations in real seismic recordings on the seabed due to the sediments and improves the model's ability to generalize across different ocean environments.

2.5 Test dataset

To evaluate the performance of our model, we conducted a comprehensive comparative analysis using distinct test datasets. Specifically, we extracted 10% of the data as test data and another 10% as

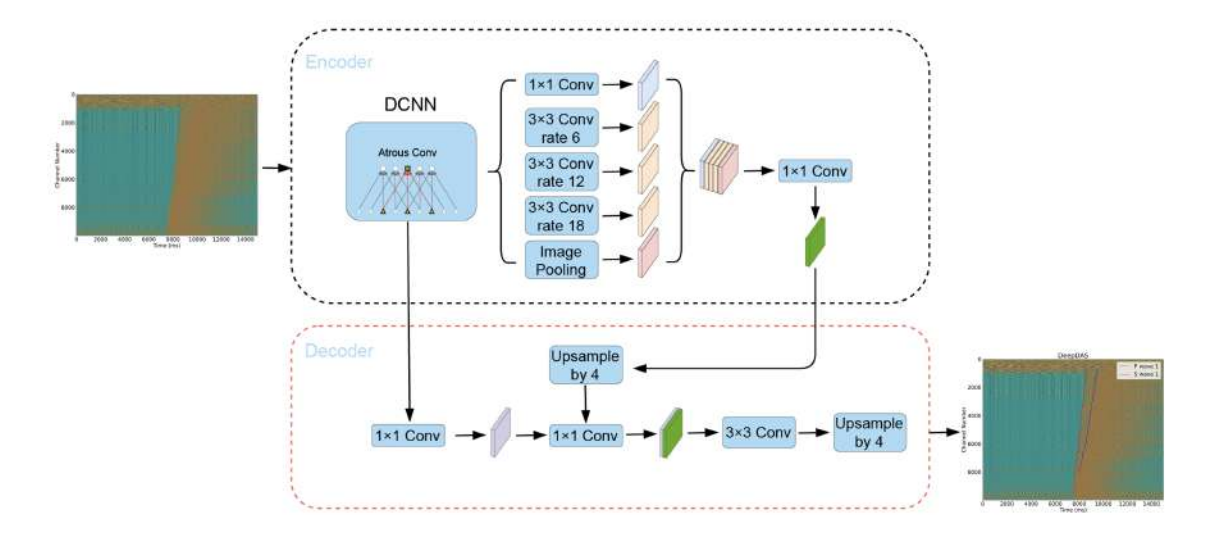


Figure 6. Architecture diagram of DeepLab v3. The model utilizes a Deep Convolutional Neural Network (DCNN) backbone (ResNet) for feature extraction, followed by an Atrous Spatial Pyramid Pooling (ASPP) module that captures contextual information at multiple scales. "Conv" denotes convolutional layers. The ASPP module combines parallel atrous (dilated) convolutions with different rates to effectively enlarge the receptive field without increasing the number of parameters. A final decoder module refines the output predictions, enabling accurate phase localization in noisy DAS data.

validation data. These subsets were randomly selected from the different DAS datasets to ensure a diverse representation, capturing a wide range of seismic event characteristics and environmental conditions. By including data from multiple regions and varying signal qualities, this approach enables a robust and generalized evaluation of the model's ability to detect seismic events under different circumstances. The random selection helps mitigate any biases that might arise from overfitting to specific subsets of the data, thus ensuring that the model's performance is a reliable reflection of its real-world applicability.

2.6 Model

We utilized the DeepLab model for our machine learning approach. DeepLab is a state-of-the-art deep learning model designed specifically for semantic image segmentation, where the goal is to classify each pixel in an image into predefined categories (Chen et al. (2017)). It leverages several advanced techniques to achieve high accuracy in segmenting complex images. One of the core innovations in DeepLab is the use of atrous convolutions, which allows the model to capture multi-scale contextual information without losing resolution (Fig. 6). This technique effectively increases the receptive field of the network without adding extra parameters, making it particularly powerful for handling varied and complex input data.

We believe that atrous convolutions are especially well-suited for processing different DAS data, as each DAS setup can have different channel spacings. By leveraging atrous convolutions, DeepLab

can better accommodate these variations in channel spacing, leading to improved performance and adaptability in analyzing diverse DAS seismic datasets. Another key feature of DeepLab is its use of the fully connected conditional random field (CRF) as a post-processing step, which refines the boundaries of segmented objects, making them more precise and better aligned with actual object contours. The model also benefits from employing backbone networks like ResNet, which enhance its ability to learn deep and rich feature representations. Due to these innovations, DeepLab has demonstrated exceptional performance in image segmentation tasks across various challenging datasets.

3 TRAINING

We pre-trained our model using terrestrial DAS data from Ridgecrest, California (761 earthquakes and 6,316,300 records), capitalizing on the similarities in seismic signal characteristics (Zhu et al. (2023); AI4EPS (2023)). Labeling this training data was also accomplished using our semi-automated labeling tool, ensuring the accuracy and consistency of the dataset. This pre-training step is crucial, as it enables the model to rapidly learn the fundamental aspects of earthquake detection, such as identifying and labeling P and S waves, providing a strong foundation that can be effectively transferred to the more challenging task of submarine seismic detection.

To adapt the DeepLab framework for DAS data, we modified its architecture to accommodate single-channel two-dimensional inputs, representing the spatiotemporal features of DAS seismic data (instead of 3 channels in image analysis). The output layer was reconfigured to classify each input segment into one of three categories: P waves, S waves, and noise. We tried different methods and found that this approach achieved the fastest training speed and the best convergence. This adjustment ensures that the model is specifically optimized for the characteristics of DAS datasets, which differ significantly from traditional three-component seismic data but also pose different structures than required in classic image analysis. For labeling P and S wave arrivals, we represent them using Gaussian functions, transforming each arrival into a probability distribution. This Gaussian representation allows for more flexible and probabilistic handling of arrival times compared to a single-point label. We can adjust the values of σ independently in both the x- and y-directions to control the width of the Gaussian distribution based on their specific needs. A smaller σ will produce a sharper, more precise peak, while a larger σ provides a broader and more tolerant representation of the arrival time. We use a larger σ in the early stages of training to help better convergence, and a smaller σ in the later stages of training to achieve higher precision.

We implemented a cross-entropy loss function, which is well-suited for classification tasks and effectively measures the divergence between the predicted probabilities and the true labels. To optimize the learning process, we employed the Adam optimizer (Diederik) (2014)), known for its adaptive

learning rate capabilities, which helps to accelerate convergence while minimizing the risk of overshooting the optimal solution.

To further enhance model robustness and generalization, we applied data augmentation techniques mentioned before during training. These included adding real seismic noise to the DAS signals, slight temporal stretching and compression, and introducing temporal shifts. Specifically, the temporal shifts were implemented by randomly selecting the starting point of the input time window within the 10-second interval preceding the P wave arrival. The shifts followed a uniform distribution and were generated once per patch based on the first channel, then applied consistently across all channels within that patch to preserve spatial coherence. These augmentations ensured that the model was exposed to a wide range of conditions, preparing it to handle diverse and noisy submarine seismic data effectively.

Initially, we set the learning rate to 1×10^{-3} for the first five epochs to facilitate rapid learning during the early training phase. After this initial period, we reduced the learning rate to 1×10^{-5} for the subsequent 20 epochs, allowing for more fine-tuned adjustments as the model converged.

Additionally, we implemented a spatial dropout rate of 0.2 to prevent overfitting by randomly deactivating a portion of the units during training. This technique improves the robustness of the model by encouraging it to learn more general features. To further mitigate the risk of over-fitting, we also implemented an early stopping mechanism that monitors the model's performance on the validation set (Prechelt (2002)). This mechanism halts training when the validation loss begins to increase, ensuring that the model retains its ability to generalize well to unseen data.

For the main training phase, we utilized 4 NVIDIA A100 GPUs, each equipped with 80 GB of memory, providing substantial computational power and memory capacity to facilitate the efficient processing of large datasets. It is worth noting that during inference, the model does not require four A100 GPUs; a single A100 or even a GPU with lower memory capacity is sufficient to execute the model. The training lasted 24 hours. During this period, we monitored various performance metrics and made adjustments as necessary to ensure the model's convergence and generalization capabilities.

4 PERFORMANCE EVALUATION

We evaluated our model's performance using recall, precision, and F1 score. The formulas for these metrics are as follows:

$$Precision = \frac{TP}{TP + FP}$$

where TP is the number of true positives and FP is the number of false positives.

$$Recall = \frac{TP}{TP + FN}$$

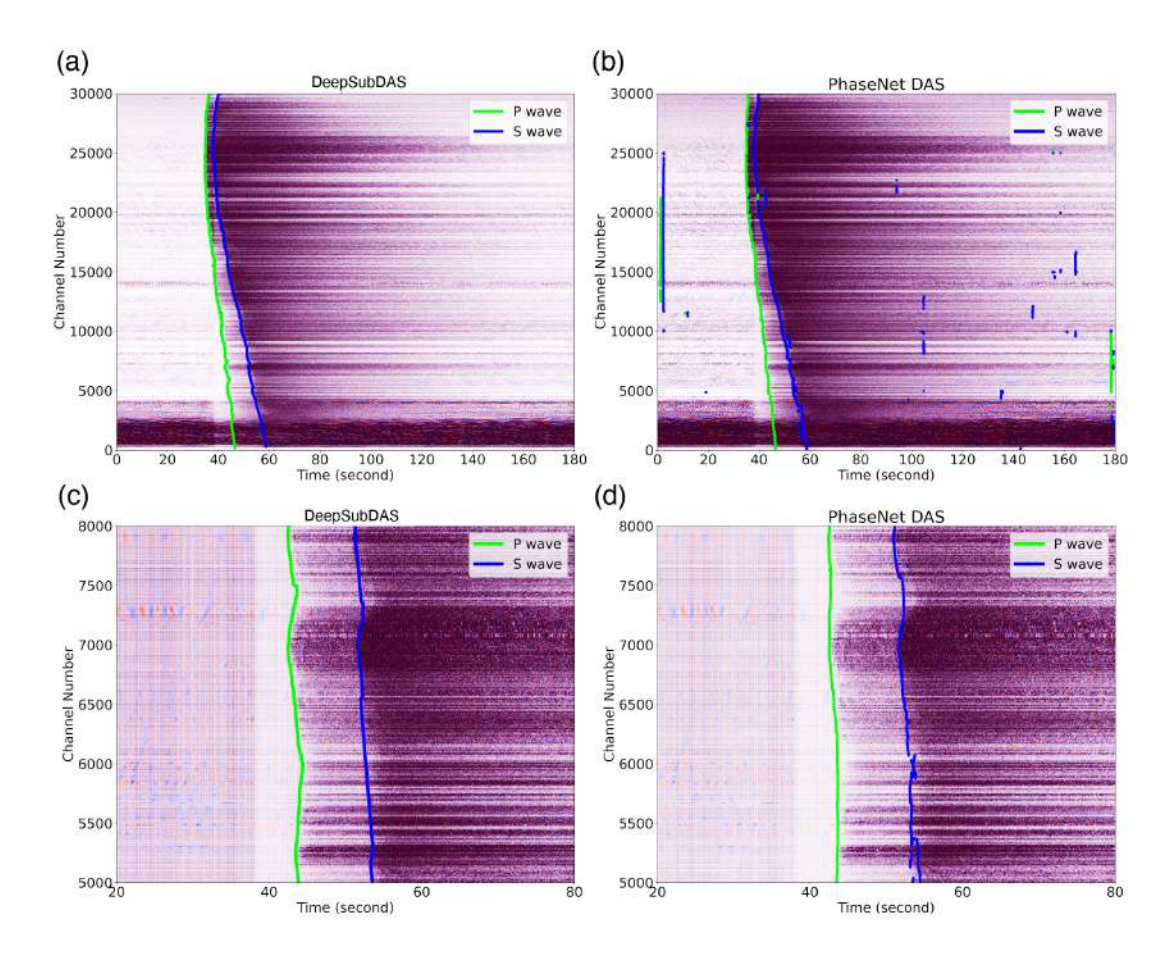


Figure 7. This figure compares the performance of DeepSubDAS (a) and PhaseNet DAS (b) in picking P and S waves for an ML 3.6 earthquake in Chile. Panels (c) and (d) provide a zoomed-in view of the results for channels 5000 to 8000.

where FN is the number of false negatives.

$$F1 = 2 \times \frac{\text{Precision} \times \text{Recall}}{\text{Precision} + \text{Recall}}$$

These metrics provide a comprehensive evaluation of the model's ability to correctly identify positive instances.

The test results for Chile, Alaska, and the rest data are summarized in Table 2 when the threshold is set to 0.8. For P wave detection in the Chilean dataset, the model achieved a precision of 0.95 and a recall of 0.93, significantly outperforming its performance on the remaining data (approximately 0.8 for both metrics). This improved performance may be attributed to the relatively larger earthquake magnitudes in the Chilean region and the noisier data in the Alaska region, which is more affected by the local storms. These factors result in more distinct and easily identifiable P-wave onsets. For S wave detection, the model exhibited consistent performance across different regions, with precision,

Region	Phase	Precision	Recall	F1	MAE (s)	Outlier (%)
Chile	P	0.95	0.93	0.94	0.22	3.2
	S	0.96	0.82	0.88	0.15	2.1
Alaska	P	0.88	0.79	0.83	0.21	4.2
	S	0.91	0.89	0.90	0.18	3.7
Rest Data	P	0.87	0.76	0.81	0.20	6.2
	S	0.88	0.85	0.86	0.17	7.1

Table 2. Performance comparison on Chilean and Alaskan coastal data. Outliers are defined as picks with absolute error > 1 second.

recall, and F1 scores all around 0.88. This indicates that the model is relatively robust in identifying S waves, regardless of regional variations in earthquake characteristics.

In addition, we compared the performance of DeepSubDAS and (original) PhaseNet DAS in picking seismic P and S waves from submarine DAS data (see Fig. 7). Our findings suggest that DeepSubDAS outperforms PhaseNet DAS in those examples. This result is understandable, as PhaseNet DAS was originally trained on DAS seismic data from land-based sources. PhaseNet DAS tends to exhibit a higher rate of false picks, which could be attributed to the differences in noise characteristics between marine DAS seismic data and those from terrestrial environments. It is worth noting that for the correctly picked P and S waves by PhaseNet DAS (Fig. 8) Table S1), the picking error is slightly higher than that of DeepSubDAS (Fig. 9), with most errors within 0.5 s. This indicates that, although PhaseNet DAS tends to produce many more false positive detections, the time error of its true positive picks remains within a reasonable range; however, there are still many outliers.

In the case of the Alaska dataset, PhaseNet DAS produced erroneous picks for both P and S waves (Fig. S1 and Table S1). The inaccuracies in picking P and S waves for the Alaska dataset are likely due to the short duration of the pre-event noise data. A longer time series of background seismic noise prior to the event could provide more contextual information, potentially benefiting the performance of both models. This difference in performance highlights the importance of training models specifically for the domain in which they will be applied, as well as the need for more diverse ocean-based training datasets to improve robustness.

Moreover, we observed that DeepSubDAS is more sensitive to local time variations caused by seafloor sediment layers, whereas PhaseNet DAS tends to produce smoother picks (Fig. 7). PhaseNet DAS's tendency toward smooth picks could be beneficial in more stable environments but becomes a disadvantage in complex, sediment-heavy seafloor regions where abrupt time delays or scattering may occur and should be visible in the picking time.

In addition, we found that DeepSubDAS is capable of detecting some signals with low SNRs that humans might miss (Fig. S2). Additionally, for some low SNR seismic records, DeepSubDAS outperforms semi-automated manual labeling (Fig. S3a and S3b). This advantage likely arises from the interpolation methods used in semi-automated labeling, which can result in significant onset deviations

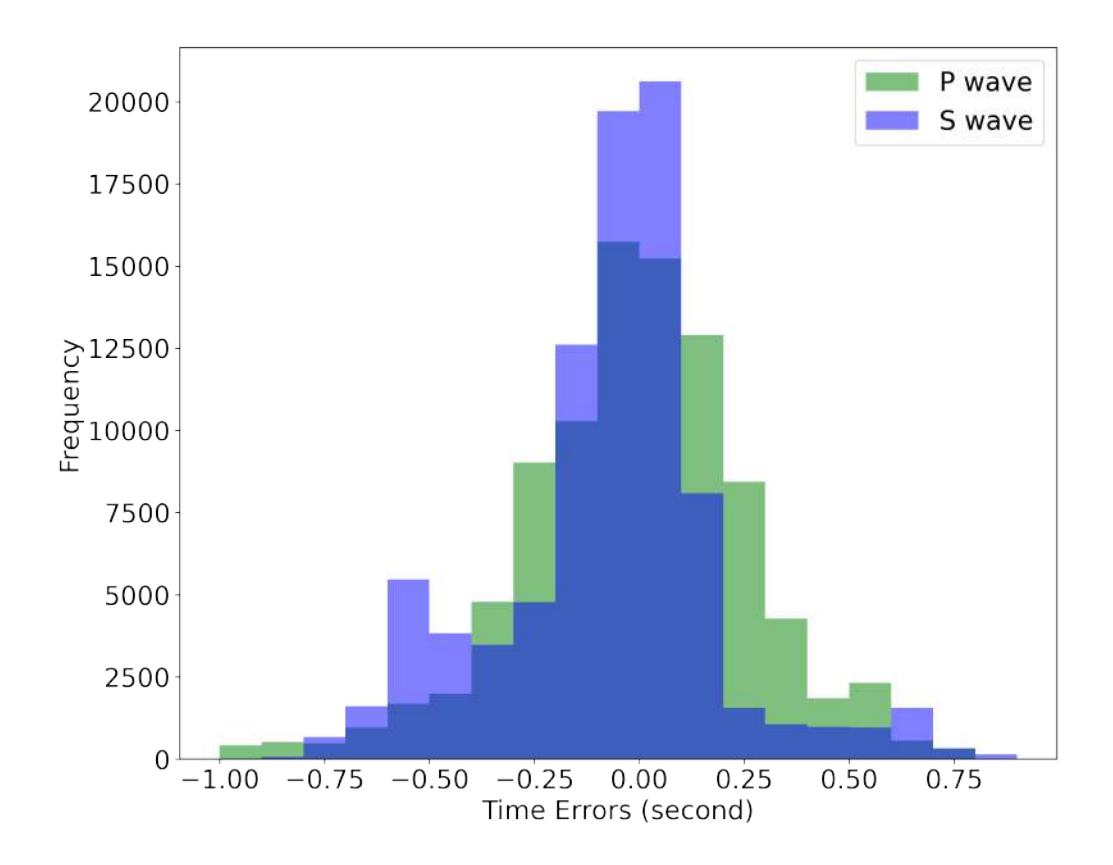


Figure 8. Histogram of P and S wave residuals of PhaseNet DAS on Alaska and Chilly data picks compared to semi-automatic picks.

in low SNR conditions, while human analysts struggle to correct these inaccuracies effectively. Furthermore, human fatigue during the labeling of large datasets can introduce errors (Fig. S3c and S3d), which further highlights the model's stability and reliability, especially in challenging data conditions.

To further elaborate on these observations, it's worth noting that the enhanced performance of DeepSubDAS may stem from its architecture being better adapted to handling the unique propagation characteristics of seismic waves in underwater environments. The marine environment introduces additional complexity, such as varying acoustic waves and noise patterns from ocean currents or biological activity, which can challenge models trained on terrestrial data.

5 DISCUSSION

While the overall performance of DeepSubDAS demonstrates clear advantages over PhaseNet DAS on submarine DAS data, several limitations and edge-case behaviors merit further discussion. These

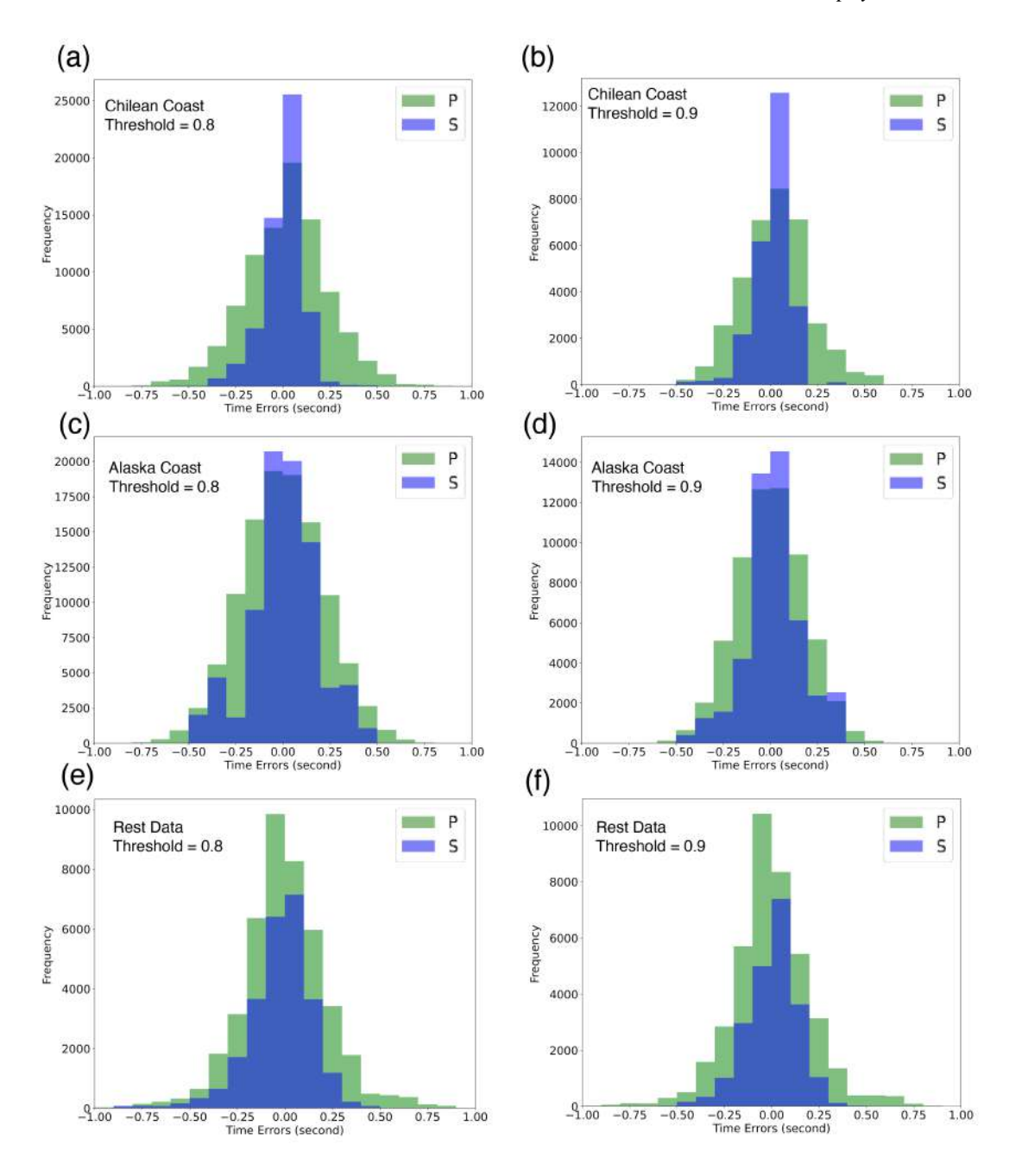


Figure 9. Histogram of P and S residuals of DeepSubDAS picks compared to semi-automatic picks. (a) and (b) show data from the Chilean coast, while (c) and (d) display data from Alaska, (e) and (f) are rest of the data. In (a), (c) and (e), the threshold we selected is 0.8, whereas in (b), (d) and (f) it is 0.9. It can be observed that the picking error follows a Gaussian distribution and is mostly within 0.2 seconds. See Table 2 for statistics of the distributions.

insights not only help clarify the current boundaries of the model but also provide directions for future development.

1. Trade-off between context window and memory constraints. When running inference on systems with limited memory, processing long time-series data across thousands of channels (e.g., 5000

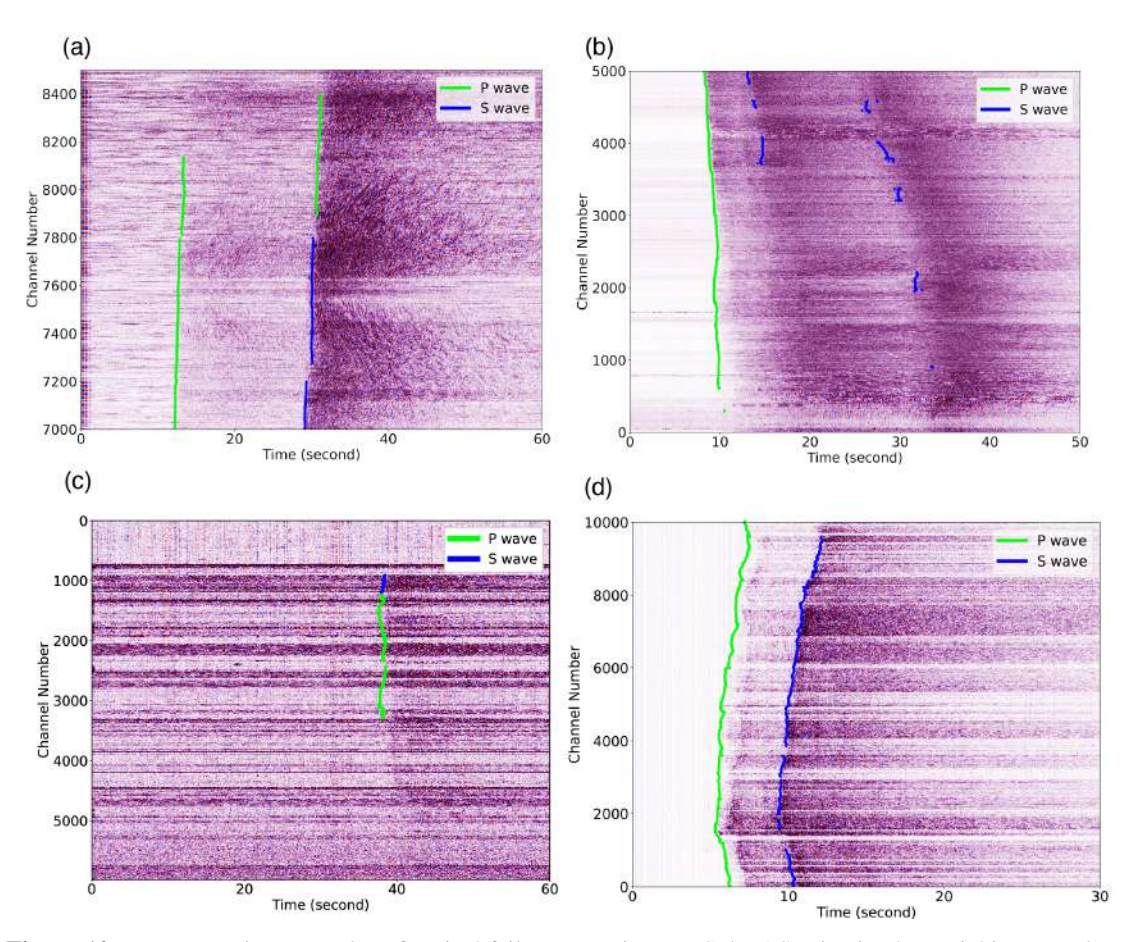


Figure 10. Representative examples of typical failure cases in DeepSubDAS seismic phase picking on submarine DAS data. (a) Limited context misclassification: In distal regions of the DAS array, where SNR is low for P waves, the model incorrectly classifies S waves as P waves due to the absence of global context when inference is limited to smaller channel subsets. (b) Obscured S wave onsets: The trailing energy of strong P wave arrivals can mask the onset of S waves, leading to incomplete or inaccurate S wave picks. (c) Severe low-SNR scenario: When the P wave signal is below the visibility threshold for both human analysts and the model, DeepSubDAS tends to label the dominant visible wave—likely the S wave—as a P wave, highlighting the model's sensitivity to amplitude in the absence of clear P phase cues. (d) Undetected converted phases: Converted phases such as PS are not identified by the model, as they are not labeled in the training dataset, which only includes P and S phases.

channels for 30 seconds) may exceed available memory. To mitigate this, we allow users to specify a smaller number of channels or shorter time windows for input. While effective in avoiding memory issues, this approach introduces a drawback: the model's limited global context. In DAS data, SNR often degrades at the cable's distal ends. In such scenarios, S wave arrivals are occasionally misclassified as P waves due to the weak P wave signals. This type of misclassification is more prevalent in single-component DAS recordings compared to traditional three-component seismometers, where polarization information aids in phase identification (see Fig. 10a).

2. Challenges in S wave onset detection. In some cases, the onset of S wave is difficult to pick accurately. This typically occurs when the coda energy from the P wave masks the beginning of the S

wave, leading to a decreased SNR for S wave identification (see Fig. 10b). These edge cases illustrate the need for improved phase boundary discrimination, especially under overlapping waveforms.

- 3. Performance under extremely low SNR conditions. Finally, in cases where the P wave signal is almost imperceptible to human analysts across the entire DAS array, the model may also fail to reliably identify the P wave. Interestingly, under such conditions, the model tends to label the only clearly visible waveform as a P wave, even when it is more likely to be an S wave due to its higher amplitude. This behavior contrasts with human analysts, who can draw on domain-specific knowledge—such as typical amplitude differences between seismic phases to make more accurate judgments (see Fig. 10c). This highlights both the model's sensitivity to phase order features and its current limitations in reliably distinguishing phases under extreme noise.
- 4. Limitations of the current training dataset Our current model is trained exclusively on manually labeled P and S phases, without inclusion of converted phases such as P-S or S-P. Consequently, the model is unable to detect or classify these converted phases (see Fig. 10t). This limitation arises not only from the training data itself but also from the model's output design, which currently considers only three classes: P, S, and noise. Properly addressing converted phases would require either extending the classification scheme to include P-S and S-P phases or training separate models specialized for converted phases. Given the prevalence and often large amplitude of converted phases—particularly P-S conversions—this limitation is important to acknowledge. A more diverse and fully annotated dataset that includes these phases would likely enhance the model's versatility and interpretability.

These observations emphasize that while DeepSubDAS performs robustly in many settings, its behavior is still influenced by architectural constraints, input preprocessing strategies, and the composition of the training dataset. Particularly, model generalization could benefit significantly from enriched datasets that include converted phases and broader signal conditions.

6 CONCLUSIONS

In this study, we developed and trained a deep learning model specifically for submarine DAS data using a framework based on DeepLab. To support model training, we collected a dataset of 92 million seismic records from DAS data across 13 submarine fiber optic cables worldwide. Recognizing the challenge of creating a high-quality labeled dataset, we developed a semi-automated labeling tool to accurately mark P and S waves within this extensive dataset. Our model demonstrates superior performance compared to existing models, achieving higher accuracy in picking seismic P and S waves. For seismic records with low SNR ratios, it can detect arrivals, when human identification becomes difficult at best. To assert the quality of picks in such very low SNR ratios requires estimates of their performance in downstream location tasks, and is beyond the scope of the present study.

This advancement is particularly valuable for the future application of submarine DAS data in

seismic early warning systems, as it enhances both the reliability and speed of seismic event detection in underwater environments.

In this study, we did not perform earthquake relocation for two primary reasons: first, the precise locations of DAS channels along the cables were unavailable; second, relocation is not within the scope of this paper. Oceanic sediment layers, in particular, can heavily influence seismic velocities, adding complexity to precise relocation efforts.

Our model is designed with high flexibility, allowing it to process input data of varying sizes, making it well-suited for deployment across DAS datasets from different regions. This adaptability is critical for the scalability of submarine seismic monitoring, enabling more comprehensive and tailored data analysis for diverse oceanic environments. Its ability to accommodate regional variability without extensive reconfiguration underscores the model's potential as a robust tool for global submarine seismic monitoring and earthquake early warning systems.

Looking to the future, several strategies can be employed to improve the generalization and accuracy of our model. One key approach is the adoption of advanced deep learning architectures, such as combining convolution networks with recurrent or transformer models, which can enhance the model's ability to capture both spatial and temporal patterns in seismic data. Furthermore, data augmentation techniques and the generation of synthetic data could help expand the training dataset, allowing the model to generalize over a wider range of seismic events and noise conditions. To further improve the adaptability of the model, we can explore multisource data fusion, integrating submarine DAS data with complementary sensors such as ocean bottom seismometers or satellite-based measurements. Furthermore, transfer learning and domain adaptation techniques would allow the model to be more easily adapted to new regions with fewer available data. Finally, expanding the dataset to include a wider variety of seismic events from different geographic and geological conditions will ensure the model's robustness, allowing it to perform reliably in diverse underwater environments. Through these advances, our goal is to create a more accurate, flexible, and scalable tool for submarine seismic monitoring and rapid earthquake detection systems.

REFERENCES

AI4EPS, 2023. quakeflow das (revision 91b72d3), hugging face.

Bornstein, T., Lange, D., Münchmeyer, J., Woollam, J., Rietbrock, A., Barcheck, G., Grevemeyer, I., & Tilmann, F., 2024. Pickblue: Seismic phase picking for ocean bottom seismometers with deep learning, *Earth and Space Science*, **11**(1), e2023EA003332.

Bouffaut, L., Taweesintananon, K., Kriesell, H. J., Rørstadbotnen, R. A., Potter, J. R., Landrø, M., Johansen, S. E., Brenne, J. K., Haukanes, A., Schjelderup, O., & Storvik, F., 2022. Eavesdropping at the speed of light: Distributed acoustic sensing of baleen whales in the arctic, *Frontiers in Marine Science*, 9.

Chen, L.-C., Papandreou, G., Kokkinos, I., Murphy, K., & Yuille, A. L., 2017. Deeplab: Semantic image

- segmentation with deep convolutional nets, atrous convolution, and fully connected crfs, *IEEE transactions* on pattern analysis and machine intelligence, **40**(4), 834–848.
- Diederik, K., 2014. Adam: A method for stochastic optimization, arXiv.
- Jousset, P., Reinsch, T., Ryberg, T., Blanck, H., Clarke, A., Aghayev, R., Hersir, G. P., Henninges, J., Weber, M., & Krawczyk, C. M., 2018. Dynamic strain determination using fibre-optic cables allows imaging of seismological and structural features, *Nature communications*, 9(1), 2509.
- Latorre, H., Ventosa, S., Ugalde, A., Villaseñor, A., Bartolomé, R., & Ranero, C. R., 2025. Kvp: a multiscale kurtosis approach for seismic phase picking, *Geophysical Journal International*, **241**(3), 1923–1935.
- Lindsey, N. J., Martin, E. R., Dreger, D. S., Freifeld, B., Cole, S., James, S. R., Biondi, B. L., & Ajo-Franklin, J. B., 2017. Fiber-optic network observations of earthquake wavefields, *Geophysical Research Letters*, 44(23), 11,792–11,799.
- Lindsey, N. J., Dawe, T. C., & Ajo-Franklin, J. B., 2019. Illuminating seafloor faults and ocean dynamics with dark fiber distributed acoustic sensing, *Science*, **366**(6469), 1103–1107.
- Lior, I., Rivet, D., Ampuero, J.-P., Sladen, A., Barrientos, S., Sanchez-Olavarria, R., Villarroel Opazo, G. A., & Bustamante Prado, J. A., 2023. Magnitude estimation and ground motion prediction to harness fiber optic distributed acoustic sensing for earthquake early warning, *Scientific Reports*, **13**(1), 424.
- Loureiro, A., Schlaphorst, D., Matias, L., Pereira, A., Corela, C., Gonçalves, S., & Caldeira, R., 2025. Non-peer reviewed report submitted to first das observations from the geolab fibre in madeira, portugal, *Authorea Preprints*.
- Mata Flores, D., Mercerat, E. D., Ampuero, J. P., Rivet, D., & Sladen, A., 2023. Identification of two vibration regimes of underwater fibre optic cables by distributed acoustic sensing, *Geophysical Journal International*, **234**(2), 1389–1400.
- Mousavi, S. M., Zhu, W., Sheng, Y., & Beroza, G. C., 2019. Cred: A deep residual network of convolutional and recurrent units for earthquake signal detection, *Scientific reports*, **9**(1), 10267.
- Mousavi, S. M., Ellsworth, W. L., Zhu, W., Chuang, L. Y., & Beroza, G. C., 2020. Earthquake transformer—an attentive deep-learning model for simultaneous earthquake detection and phase picking, *Nature communications*, **11**(1), 3952.
- Münchmeyer, J., Woollam, J., Rietbrock, A., Tilmann, F., Lange, D., Bornstein, T., Diehl, T., Giunchi, C., Haslinger, F., Jozinović, D., et al., 2022. Which picker fits my data? a quantitative evaluation of deep learning based seismic pickers, *Journal of Geophysical Research: Solid Earth*, **127**(1), e2021JB023499.
- Ni, Y., Denolle, M. A., Shi, Q., Lipovsky, B. P., Pan, S., & Kutz, J. N., 2024. Wavefield reconstruction of distributed acoustic sensing: Lossy compression, wavefield separation, and edge computing, *Journal of Geophysical Research: Machine Learning and Computation*, **1**(3), e2024JH000247.
- Niksejel, A. & Zhang, M., 2024. OBSTransformer: a deep-learning seismic phase picker for OBS data using automated labelling and transfer learning, *Geophysical Journal International*, **237**(1), 485–505.
- Posey, R., Johnson, G., & Vohra, S., 2000. Strain sensing based on coherent rayleigh scattering in an optical fibre, *Electronics Letters*, **36**, 1688–1689.
- Prechelt, L., 2002. Early stopping-but when?, in *Neural Networks: Tricks of the trade*, pp. 55–69, Springer. Romanowicz, B., Allen, R., Brekke, K., Chen, L., Gou, Y., Henson, I., Marty, J., Neuhauser, D., Pardini, B.,

- Taira, T., Thompson, S., Zhang, J., & Zuzlewski, S., 2023. SeaFOAM: A Year-Long DAS Deployment in Monterey Bay, California, *Seismological Research Letters*, **94**(5), 2348–2359.
- Ruppert, N. A., Barcheck, G., & Abers, G. A., 2022. Enhanced Regional Earthquake Catalog with Alaska Amphibious Community Seismic Experiment Data, *Seismological Research Letters*, **94**(1), 522–530.
- Shi, Q. & Denolle, M. A., 2023. Improved observations of deep earthquake ruptures using machine learning, *Journal of Geophysical Research: Solid Earth*, **128**(12), e2023JB027334.
- Shi, Q., Denolle, M. A., Ni, Y., Williams, E. F., & You, N., 2025. Denoising offshore distributed acoustic sensing using masked auto-encoders to enhance earthquake detection, *Journal of Geophysical Research: Solid Earth*, **130**(2), e2024JB029728.
- Sladen, A., Rivet, D., Ampuero, J. P., De Barros, L., Hello, Y., Calbris, G., & Lamare, P., 2019. Distributed sensing of earthquakes and ocean-solid earth interactions on seafloor telecom cables, *Nature communications*, **10**(1), 5777.
- Spica, Z. J., Nishida, K., Akuhara, T., Pétrélis, F., Shinohara, M., & Yamada, T., 2020. Marine sediment characterized by ocean-bottom fiber-optic seismology, *Geophysical Research Letters*, **47**(16), e2020GL088360, e2020GL088360 10.1029/2020GL088360.
- Spica, Z. J., Ajo-Franklin, J., Beroza, G. C., Biondi, B., Cheng, F., Gaite, B., Luo, B., Martin, E., Shen, J., Thurber, C., Viens, L., Wang, H., Wuestefeld, A., Xiao, H., & Zhu, T., 2023. PubDAS: A PUBlic Distributed Acoustic Sensing Datasets Repository for Geosciences, *Seismological Research Letters*, **94**(2A), 983–998.
- Strumia, C., Trabattoni, A., Supino, M., Baillet, M., Rivet, D., & Festa, G., 2024. Sensing optical fibers for earthquake source characterization using raw das records, *Journal of Geophysical Research: Solid Earth*, **129**(1), e2023JB027860.
- Trabattoni, A., Vernet, C., van den Ende, M., Baillet, M., Potin, B., & Rivet, D., 2024. Sediment corrections for distributed acoustic sensing.
- Tsuji, T., Ikeda, T., Matsuura, R., Mukumoto, K., Hutapea, F. L., Kimura, T., Yamaoka, K., & Shinohara, M., 2021. Continuous monitoring system for safe managements of co2 storage and geothermal reservoirs, *Scientific reports*, **11**(1), 19120.
- Ugalde, A., Becerril, C., Villaseñor, A., Ranero, C. R., Fernández-Ruiz, M. R., Martin-Lopez, S., González-Herráez, M., & Martins, H. F., 2021. Noise Levels and Signals Observed on Submarine Fibers in the Canary Islands Using DAS, *Seismological Research Letters*, **93**(1), 351–363.
- van den Ende, M., Trabattoni, A., Baillet, M., & Rivet, D., 2025. An analysis of the dynamic range of distributed acoustic sensing for earthquake early warning, *Seismica*, **4**(1).
- Wilcock, W. S. D., Abadi, S., & Lipovsky, B. P., 2023. Distributed acoustic sensing recordings of low-frequency whale calls and ship noise offshore Central Oregon, *JASA Express Letters*, **3**(2), 026002.
- Williams, E. F., Ugalde, A., Martins, H. F., Becerril, C. E., Callies, J., Claret, M., Fernandez-Ruiz, M. R., Gonzalez-Herraez, M., Martin-Lopez, S., Pelegri, J. L., Winters, K. B., & Zhan, Z., 2023. Fiber-optic observations of internal waves and tides, *Journal of Geophysical Research: Oceans*, **128**(9), e2023JC019980.
- Withers, M., Aster, R., Young, C., Beiriger, J., Harris, M., Moore, S., & Trujillo, J., 1998. A comparison of select trigger algorithms for automated global seismic phase and event detection, *Bulletin of the Seismological Society of America*, **88**(1), 95–106.

Woollam, J., Münchmeyer, J., Tilmann, F., Rietbrock, A., Lange, D., Bornstein, T., Diehl, T., Giunchi, C., Haslinger, F., Jozinović, D., et al., 2022. Seisbench—a toolbox for machine learning in seismology, *Seismological Society of America*, **93**(3), 1695–1709.

Xiao, H., 2025. Deepsubdas: An earthquake phase picker from submarine distributed acoustic sensing data, [Dataset] Zenodo.

Xiao, H., Tanimoto, T., Spica, Z. J., Gaite, B., Ruiz-Barajas, S., Pan, M., & Viens, L., 2022. Locating the precise sources of high-frequency microseisms using distributed acoustic sensing, *Geophysical Research Letters*, **49**(17), e2022GL099292.

Xiao, H., Spica, Z. J., Li, J., & Zhan, Z., 2024. Detection of earthquake infragravity and tsunami waves with underwater distributed acoustic sensing, *Geophysical Research Letters*, **51**(2), e2023GL106767.

Yin, J., Soto, M. A., Ramírez, J., Kamalov, V., Zhu, W., Husker, A., & Zhan, Z., 2023. Real-Data Testing of Distributed Acoustic Sensing for Offshore Earthquake Early Warning, *The Seismic Record*, **3**(4), 269–277.

Yoon, C. E., O'Reilly, O., Bergen, K. J., & Beroza, G. C., 2015. Earthquake detection through computationally efficient similarity search, *Science advances*, **1**(11), e1501057.

Zhu, W. & Beroza, G. C., 2018. PhaseNet: a deep-neural-network-based seismic arrival-time picking method, *Geophysical Journal International*, **216**(1), 261–273.

Zhu, W., Biondi, E., Li, J., Yin, J., Ross, Z. E., & Zhan, Z., 2023. Seismic arrival-time picking on distributed acoustic sensing data using semi-supervised learning, *Nature Communications*, **14**(1), 8192.

Open Research Statement

The data files and code used in this paper are available at Xiao (2025). Upon potential acceptance of this manuscript, we also plan to share the trained model.

Acknowledgements

We gratefully acknowledge the support of EU-INFRATECH, Grant agreement ID: 101095055 (SUB-MERSE project). We thank Zack Spica and the co-authors of PubDAS for sharing their data. Special thanks to Zhongwen Zhan for sharing the Ridgecrest earthquake data and to Alister Trabattoni for sharing the Chilean coastline earthquake data. Additionally, we appreciate the SeisBench and DeepLab projects for providing their code. This work utilized high-performance computing resources made possible by funding from the Ministry of Science, Research and Culture of the State of Brandenburg (MWFK) and is operated by the IT Services and Operations unit of the Helmholtz Centre Potsdam. We thank GCI for providing access to submarine fibers in Cook Inlet, Alaska. The data acquisition and storage are supported by the UW FiberLab, supported by a Murdock Charitable Trust fund, and The Jerome M. Paros Endowed Chair in Sensor Networks to Dr William Wilcock at University of Washington.